

## Analysis of isotopic daughter nuclei $^{238,239}Pu$ formed via $xn$ -emission from $^{240}Pu^*$ formed in n-induced reaction

Amandeep Kaur<sup>1,\*</sup>, Jagdeep Kaur<sup>1</sup>, Gudveen Sawhney<sup>2</sup>, and Manoj K. Sharma<sup>3</sup>

<sup>1</sup>Department of Physics, School of Basic and Applied Sciences,  
RIMT University, Mandi Gobindgarh-140406, Punjab, India

<sup>2</sup>Department of Physics, University Institute of Sciences,  
Chandigarh University, Punjab-140413, India and

<sup>3</sup>School of Physics and Materials Science,  
Thapar Institute of Engineering and Technology, Patiala-147004, Punjab, India

### Introduction

The isotopes of Plutonium ( $Z=94$ ) is an interesting topic of research due to the wide area of applications.  $^{239}Pu$  is highly fissile and is used as a nuclear fuel while  $^{238}Pu$  is used in batteries of space vehicles because it decays via alpha emission and the heat generated in this radioactive decay is utilized here. Neutron evaporation analysis plays a crucial role as it opens the possibility of isotope formation from the decaying nuclear system although fission decay competes in this mass region.

The main objective of this work is to address the production cross-sections of  $^{238}Pu$  after  $2n$ -emission from the system  $^{240}Pu^*$  formed in  $n + ^{239}Pu$  reaction over three in-

ident beam energies  $E_{beam}=7.1, 7.7$  and  $9.3$  MeV in reference to an experiment performed by V. Méot et al. [1], using the dynamical approach of DCM Model [2]. These cross-sections are addressed by varying the neck-length parameter ( $\Delta R$ ) of the model, for the deformed choice of fragmentation ( $\beta_2$  deformed fragments). Within the framework of DCM, the cross-sections for light particle emission are adequately addressed via non-sticking limits of moment of inertia ( $I_{NS}$ ) as it imparts lower angular momentum ( $\ell$ ) values to the nuclear system while the fission data is fitted by sticking moment of inertia ( $I_S$ ), because of high  $\ell$ -values imparted using this approach. Hence, the present evaluation is done through  $I_{NS}$  approach, to rule out the competition from fission decay. The neck values required for the addressal of the above-mentioned data are  $1.737$  fm,  $1.40$  fm and  $1.45$  fm respectively, at  $E_{beam}=7.1, 7.7$  and  $9.3$  MeV.

### The Dynamical Cluster-decay Model (DCM)

The DCM [2] finds its origin from the QMFT and proceeds through the collective coordinates of mass (and charge) asymmetries  $\eta_A = (A_1 - A_2)/(A_1 + A_2)$  (and  $\eta_Z = (Z_1 - Z_2)/(Z_1 + Z_2)$ ) and relative separation  $R$ . The decay cross-sections for hot ( $T \neq 0$ ) and rotating ( $\ell \neq 0$ ) nucleus is given as:

$$\sigma = \frac{\pi}{k^2} \sum_{\ell=0}^{\ell_{max}} (2\ell + 1) P_0 P; k = \sqrt{\frac{2\mu E_{c.m.}}{\hbar^2}} \quad (1)$$

Here,  $P_0$  is preformation probability,  $P$  is penetrability and  $\ell_{max}$  is the maximum angular

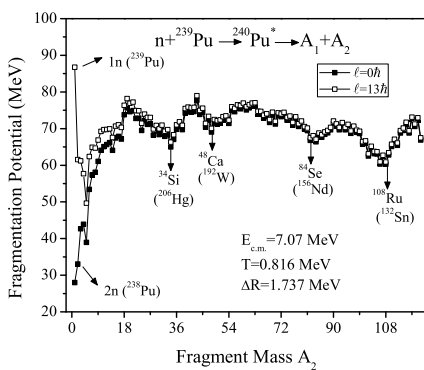


FIG. 1: Variation of fragmentation potential as a function of fragment mass ( $A_2$ ), for the decay of  $^{240}Pu^*$  plotted at  $E_{c.m.}=7.07$  MeV.

\*Electronic address: [kauramandeep@rimt.ac.in](mailto:kauramandeep@rimt.ac.in)

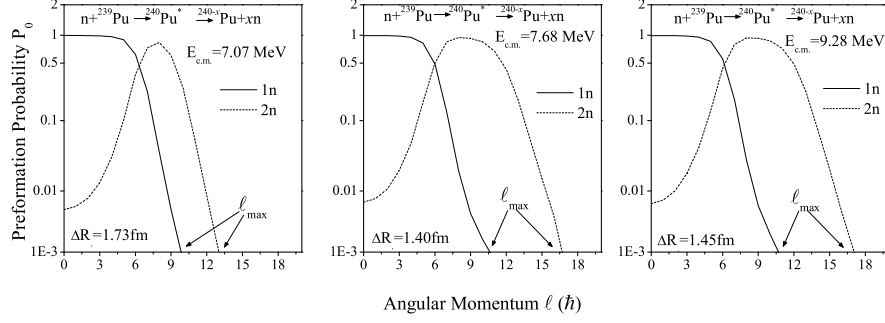


FIG. 2: Variation of preformation probability  $P_0$  as a function of angular momentum for  $1n$  and  $2n$ -emission from  $^{240}Pu^*$  at the three reported energies.

momentum fixed for the vanishing of  $xn$ -cross-sections.

## Calculations and discussions

The structural information is evident from Fig. 1, where fragmentation potential ( $V_\eta$ ) is plotted in terms of fragment mass  $A_2$  at the lowest energy  $E_{beam}=7.1$  or  $E_{c.m.}=7.07$  MeV, corresponding to extreme values of angular momentum  $\ell = 0\hbar$  and  $\ell = 13\hbar$ . The figure favors the formation of isotopic daughter nuclei  $^{238,239}Pu^*$  at  $\ell = 0\hbar$  state as the magnitude of  $V_\eta$  for  $1n$  and  $2n$  evaporation is less as compared to other fragments. Certain minimas are also marked which correspond to the fragments having lowered  $V_\eta$  values relative to their neighboring fragments. These fragments correspond to magic shell or deformed magic shell configurations. For example, the strong minima around  $A_2=108$  is attributed to the shell effects arising due to the emergence of  $^{132}Sn$  as the complementary fragment. Also, at higher  $\ell$ -states, structural variations are observed which signify an increase in the magnitude of  $V_\eta$  for  $1n$  and  $2n$ -evaporation. This is justified from the choice of the limits of moment of inertia used which is defined as  $I_{NS} = \mu R^2$ ,  $\mu$  being the reduced mass of the system. For  $1n$ -evaporation, the reduced mass of this binary decay is less than one and hence, it imparts enhanced centrifugal potential to the system. Whereas for other decays with  $A_2 \geq 2$ , the reduced mass of the binary decay goes on increasing and the corresponding value of centrifugal potential decreases. The effect of increasing  $\ell$  seems to be silent for

heavier fragments. It is important to note here that the enhanced  $V_\eta$  evinces a reduced probability of emission in the decay channel. This effect of  $\ell$  on the emission probability of  $1n$  and  $2n$  or consequently the formation probability of  $^{238,239}Pu$  daughter nuclei is clarified from Fig. 2, where  $P_0$  is plotted as a function of  $\ell$  at the three reported energies. From the Fig. 2, it is clear that the  $P_0$  values are high at lower  $\ell$ -values and then decrease to negligible values, for  $1n$ -evaporation, as suggested by Fig. 1. Moreover, for  $2n$ -evaporation the  $P_0$  values first increase with increasing  $\ell$  values and become maximum around those values of  $\ell$  at which  $(P_0)_{1n} \rightarrow 0$ . As the  $\ell$ -values are increased further, the  $(P_0)_{2n}$  starts decreasing to negligibly small values. The  $\ell$ -values corresponding to which  $(P_0)_{2n} \rightarrow 0$  is  $13\hbar$ ; least for  $E_{c.m.}=7.07$  MeV and increases to  $\ell_{max} = 17\hbar$  at higher incident energies. The lower  $\ell_{max}$  value at  $E_{c.m.}=7.07$  MeV may be associated with the relatively higher magnitude of neck parameter used while addressing  $2n$ -emission cross-sections from  $^{240}Pu^*$  at this energy.

## Acknowledgement

The financial support from CSIR, New Delhi is gratefully acknowledged.

## References

- [1] V. Méot et al., Phys. Rev. C 103, 054609 (2021).
- [2] R. K. Gupta, M. Bansal, Int. Rev. Phys. (I. RE. Phys.) 5, 74, (2011).